Smart Structures and Systems, *Vol. 15, No. 2 (2015) 469-488*
DOI: http://dx.doi.org/10.12989/sss.2015.15.2.469

Analysis of three-dimensional thermal gradients for arch bridge girders using long-term monitoring data

Guang-Dong Zhou[*1], Ting-Hua Yi[2a], Bin Chen[3b] and Huan Zhang[1c]

[1]*College of Civil and Transportation Engineering, Hohai University, Nanjing 210098, China*
[2]*School of Civil Engineering, Dalian University of Technology, Dalian 116024, China*
[3]*College of Civil Engineering and Architecture, Zhejiang University of Technology, Hangzhou 310003, China*

(Received November 7, 2014, Revised January 9, 2015, Accepted January 11, 2015)

Abstract. Thermal loads, especially thermal gradients, have a considerable effect on the behaviors of large-scale bridges throughout their lifecycles. Bridge design specifications provide minimal guidance regarding thermal gradients for simple bridge girders and do not consider transversal thermal gradients in wide girder cross-sections. This paper investigates the three-dimensional thermal gradients of arch bridge girders by integrating long-term field monitoring data recorded by a structural health monitoring system, with emphasis on the vertical and transversal thermal gradients of wide concrete-steel composite girders. Based on field monitoring data for one year, the time-dependent characteristics of temperature and three-dimensional thermal gradients in girder cross-sections are explored. A statistical analysis of thermal gradients is conducted, and the probability density functions of transversal and vertical thermal gradients are estimated. The extreme thermal gradients are predicted with a specific return period by employing an extreme value analysis, and the profiles of the vertical thermal gradient are established for bridge design. The transversal and vertical thermal gradients are developed to help engineers understand the thermal behaviors of concrete-steel composite girders during their service periods.

Keywords: structural health monitoring; thermal gradient; temperature; concrete-steel composite cross-section; arch bridge

1. Introduction

Bridges are crucial elements across rivers, lakes, canyons and straits; they form advanced transportation networks with extensive service periods that can exceed 50 years or 100 years. During their lifespans, bridges are inevitably subjected to daily, seasonal, and yearly repeated cycles of heating and cooling, which are induced by solar radiation and the surrounding air. As a result, temperature variations and thermal gradients may cause considerable thermal stress and deformation in bridge components. These thermal stresses may be comparable to the stresses caused by dead and live loads in statically indeterminate bridges, which can initiate tensile cracks

*Corresponding author, Assistant Professor, E-mail: zhougd@hhu.edu.cn
[a] Professor, E-mail: yth@dlut.edu.cn
[b] Ph.D., Student, E-mail: jeetchen_123@hotmail.com
[c] Ph.D., Student, E-mail: hhuan1214@gmail.com

http://www.techno-press.org/?journal=sss&subpage=8 ISSN: 1738-1584 (Print), 1738-1991 (Online)

in concrete bridges due to the low tensile strength of materials. Thermal deformation may cause a shift in the structural dynamic parameters and the collapse of an entire structure. According to an investigation conducted by Oesterle *et al*. (2007), the progressive collapse of the Red Mountain Freeway bridge girders was induced by the combination of lateral thermal deformations and initial imperfections and constructional errors. Therefore, thermal loads substantially affect the performance of bridges throughout their lifecycles. The failure to understand the effect of temperature can result in considerable damage to bridges and false alarms of structural deterioration (Xia *et al*. 2006).

In the early 1960s, Zuk (1965) began a study of the thermal behaviors of highway bridges. After the investigation of several bridges, the study concluded that the thermal load is affected by air temperature, wind, humidity, intensity of solar radiation, and material type. Researchers and engineers subsequently promoted comprehensive studies of thermal loads in different types of bridges, such as concrete bridges, steel bridges, and concrete-steel composite bridges using theoretical analysis, numerical simulation, and field measurement. Derived from the heat transfer equation proposed by Fourier, the boundary condition that involves the heat exchange between the boundary of a bridge and the environment was simplified and formulated by Orgill and Hollands (1977), Elbadry and Ghali (1983), and Duffie (2013). Although these achievements almost analytically solve the Fourier heat transfer equation, obtaining the closed-form solution of temperature distribution in bridge girders with complicated geometric configurations remains a challenging task. To overcome this difficulty, numerical methods including the finite difference method and the finite element method were employed. Following the one-dimensional finite-difference method developed by Potgieter and Gamble (1983), Mirambell and Aguado (1990) proposed a two-dimensional finite difference model to determine the time-dependent vertical and transverse temperature variation within the cross-section of concrete bridges. Benefitting from the rapid development of commercial finite element software, simulating the temperature distribution in various types of bridges by the finite element method was also conducted by many researchers (Fu *et al*. 1990, Moorty and Roeder 1992, Xia *et al*. 2013). Numerical simulation provides a perfect approach to predict the thermal load in a bridge with different boundary conditions, environment conditions, geometrical configurations and material properties. However, the simulated results are heavily dependent on the values of input parameters, which are difficult to determine. With the development of sensing and information technologies, on-line structural health monitoring (SHM) has gained worldwide applications in civil engineering field over the past decade (Ye *et al*. 2012, Ye *et al*. 2013). Field measurements using temperature sensors integrated in the SHM system were implemented on many bridges. The temperature data obtained from field measurements provide the most practical results of thermal loads in bridges, and the statistical analysis is employed to investigate these monitored data. Roberts-Wollman *et al*. (2002) investigated temperature data for 2 1/2 years, which had been recorded by thermocouples instrumented on a segmental concrete box girder bridge, it was reported that both the typical positive gradient curve and negative gradient curve can be approximated by a fifth-order parabola with different points of zero temperature difference. Im et al. (2004) monitored a steel-concrete composite box girder bridge located at the south of Seoul by 30 copper-constant thermocouples over a 6 years period. The extreme thermal load parameters with return periods of 50 years and 100 years, including effective temperature, vertical temperature difference and horizontal temperature difference, were predicted using the extreme value analysis (EVA) method. Li *et al*. (2004) analyzed three-year temperature data that were recorded on the Confederation Bridge using the EVA method. The results show that all the thermal variables follow a Gumbel distribution. Ni

et al. (2007) investigated one-year continuous measurement data recorded by a total of 83 temperature sensors, which had been installed at different locations of the Ting Kau Bridge in Hong Kong. The EVA was employed to estimate the extreme effective temperatures of bridge deck with a certain return period. Xu *et al*. (2010) investigated the monitored temperatures of the Tsing Ma Bridge from 1997 to 2005. Based on the measurement data, the statistics of ambient air temperature, effective temperature and displacement response of the bridge were figured out, and the statistical relationship between the effective temperature and the displacement of the bridge was established. These conclusions provide valuable knowledge about the thermal loads and thermal behaviors of bridges. An overview of current research and development activities in the field of thermal loads in bridges was presented by Zhou and Yi (2013).

Previous studies provide valuable temperature information for bridge design and evaluation. The majority of the studies focus on the vertical thermal gradient under the assumption that the heat flow across the depth of the cross-section is considerable and the transversal and longitudinal heat flow can be neglected. Wide concrete-steel composite girders, which can utilize the compression capability of concrete and the tension capability of steel and provide economic structures, are extensively adopted in long-span bridges. In a wide concrete-steel composite girder, the concrete and the steel have different heat properties, such as emissivity and absorptivity, which induces a complex and varying temperature distribution among general cases. Field measurement results indicate that notable transversal thermal gradients extensively exist in bridges with wide cross-sections and exert a critical influence on the performance of bridges. According to studies performed by Im *et al*. (2004), Lee (2012), and Ding *et al*. (2012), the transversal thermal gradient in wide cross-sections may exceed the vertical thermal gradient. Unfortunately, bridge design specifications and literature throughout the world provide no detailed recommendations about the thermal gradients for this type of girder.

This paper aims to investigate the three-dimensional thermal gradients in a wide concrete-steel composite girder using field monitoring temperature data for one year. The time-dependent and statistical characteristics of longitudinal, vertical and transversal thermal gradients are extracted, which are expected to provide a reference for the design and evaluation of bridges with this type of cross-section. The remainder of the paper is organized as follows: Section 2 briefly introduces the temperature monitoring and data preprocessing method. Section 3 describes the time-dependent variation in temperature in the cross-sections. Section 4 presents the comprehensive features of longitudinal, vertical and transversal thermal gradients including time-varying tendencies, statistical properties, extreme values with a certain return period, and the profiles of vertical thermal gradients. Conclusions are drawn in Section 5.

2. Temperature monitoring and data preprocessing

The Jiubao Bridge is a newly constructed bridge in China with a total length of 1855 m, as shown in Fig. 1. The bridge, which encompasses a dual three-lane carriageway and two hard shoulders for pedestrians, consists of a north approach bridge, a three-span arch bridge, and a south approach bridge. The north and south approach bridges use multi-span continuous structures; the span of each bridge is 85 m. The wide concrete-steel composite girder, which employs a 300-mm thick concrete slab supported by a single chamber steel box girder, is applied in the north and south approach bridges. As illustrated in Fig. 1, the diagonal braces with a space of 4.25 m in the box girder are employed to strengthen the main girder and the diagonal braces with a space of

4.25 m out of the box girder are adopted to support the cantilever concrete slab. The maximum total width of the cross-section is 31.5 m, but the depth of the cross-section is only 4.5 m. The flat geometric configuration and two dissimilar materials in the cross-section make the temperature distribution in the girder different from ordinary occasions. To completely understand the temperature distribution and thermal loads in the cross-section and to predict the thermal behaviors of the entire bridge, the temperatures of four cross-sections in the north and south approach bridges are monitored by temperature sensors. Fig. 2 plots the monitored cross-sections and the number of cross-sections. Cross-sections I and III are located at the end of the span and cross-sections II and IV are located in the middle of the span. The detailed temperature sensors locations and their numbers are shown in Fig. 3. In the figure, the top or bottom angles indicate the sensor locations. A total of 27 temperature sensors are installed. Both the concrete slab and the steel box girder are comprehensively monitored. The sensors used for monitoring temperatures in the concrete slab are embedded in the joints among different concrete slabs. The sensors used for monitoring steel temperatures are attached inside the steel box girder. All embedded temperature sensors are protected by stainless steel tubes. And all surface-type temperature sensors are placed inside customized boxes to prevent man-made disturbance, moisture and electromagnetic interference. As a result, all temperatures sensors can work reliably and sense data with high fidelity.

The temperature monitoring subsystem became operational after the completion of the north and south approach bridges in July 2011. The sampling period of the temperature sensors is set to 1 min. One year of temperature data from August 2011 to July 2012 are used in this paper. More than 500,000 records for each monitoring point were stored. The task of processing and analyzing such a large volume of data is challenging, and the efficiency of the task is unacceptable. Thus, representative data of 180 days are selected for additional research after deleting abnormal data using the criteria proposed by Xu *et al*. (2010). However, this screening has no effect on the observation of the features of thermal loads because these data are uniformly distributed over twelve months of one year and have the capability of representing temperatures for one year. Considering the reason that the temperature of structural components vary at a slow rate, these records are averaged every 10 minutes. As a result, the temperatures for one day are reduced to 144 representative samples and 25920 samples of each monitoring point are retained.

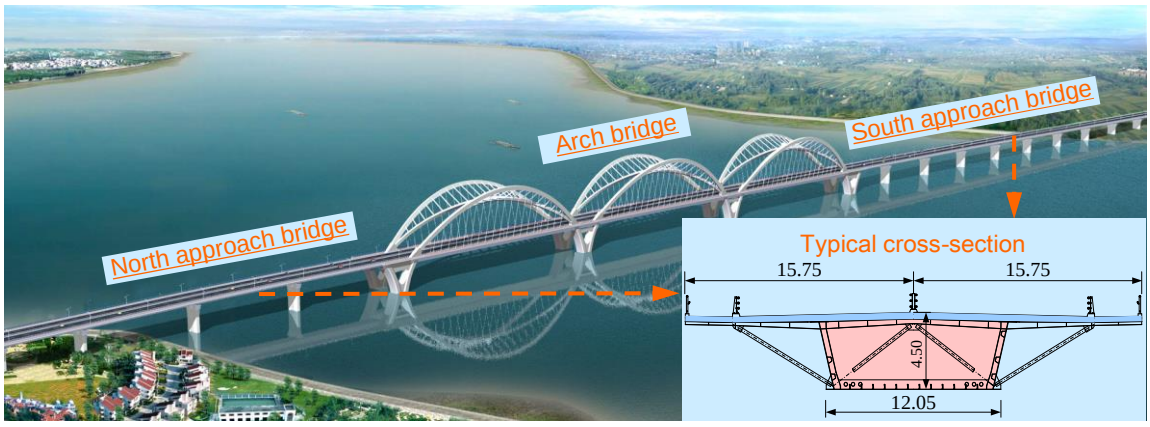

Fig. 1 Jiubao Bridge (unit: m)

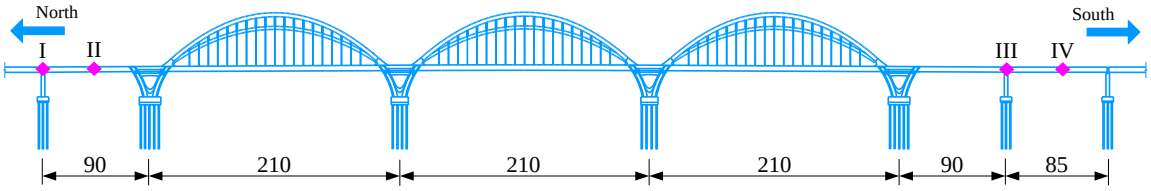

Fig. 2 Cross-sections for temperature monitoring (unit: m)

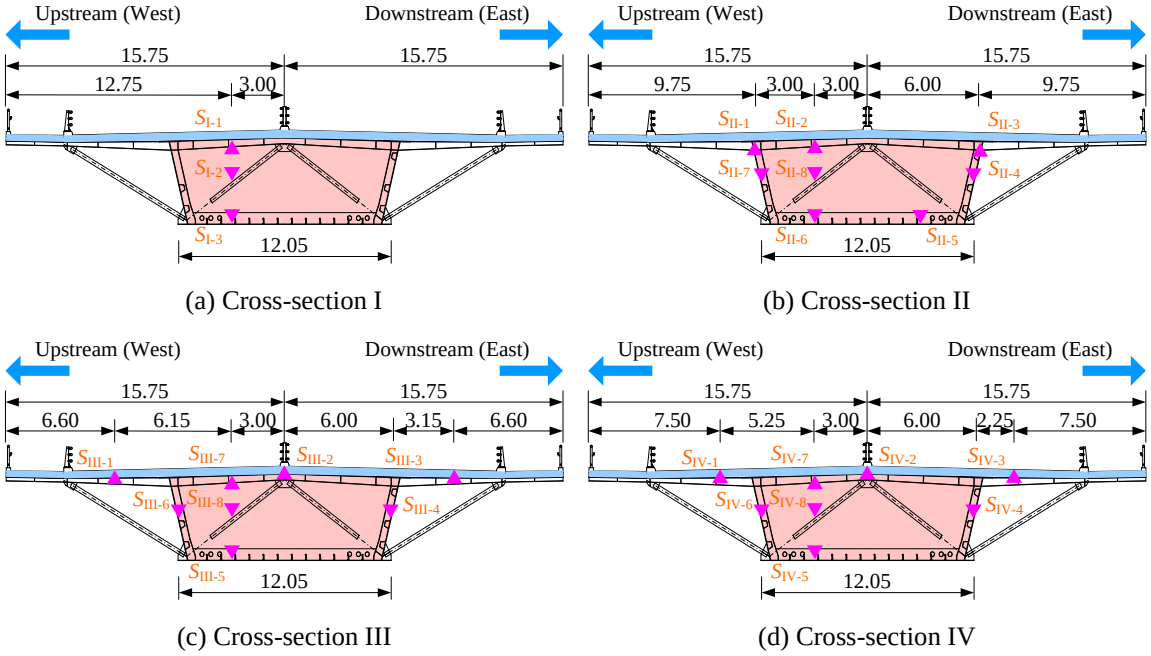

(a) Cross-section I

(b) Cross-section II

(c) Cross-section III

(d) Cross-section IV

Fig. 3 Locations and number of temperature sensors in cross-sections (unit: m)

3. Temperature in cross-sections

The Daily and monthly temperature fluctuations may induce continuous expansion and contraction of structural components and damage critical bridge members, such as expansion joints, bearings and anchor heads (Ni *et al*. 2007). The time-dependent temperatures can be used to predict the extreme values of thermal loads for bridge design and assessment. In this section, time-dependent temperatures including point temperatures, effective temperatures and daily temperature variation are investigated.

3.1 Point temperature

In each monitoring cross-section, two test points located at the top of the cross-section and the

bottom of the cross-section, respectively, are selected. The time histories of 10-min averaged temperatures in selected test points are plotted in Fig. 4. Because only 50% of the data are selected from the records for one year, as mentioned in Section 2, the curves are not continuous. As shown by the four figures in Fig. 4, the yearly temperature variation is notable. The highest temperatures emerge in July, August and September, whereas the lowest temperatures occur in January, February, March and early April. The highest and lowest temperature of the year is 50.0℃ and 1.7℃, respectively. The time histories indicate high daytime temperatures and low nighttime temperatures. These findings conclude that the structural temperatures in a bridge are highly dependent on the air temperature and exhibit a strong relationship with time.

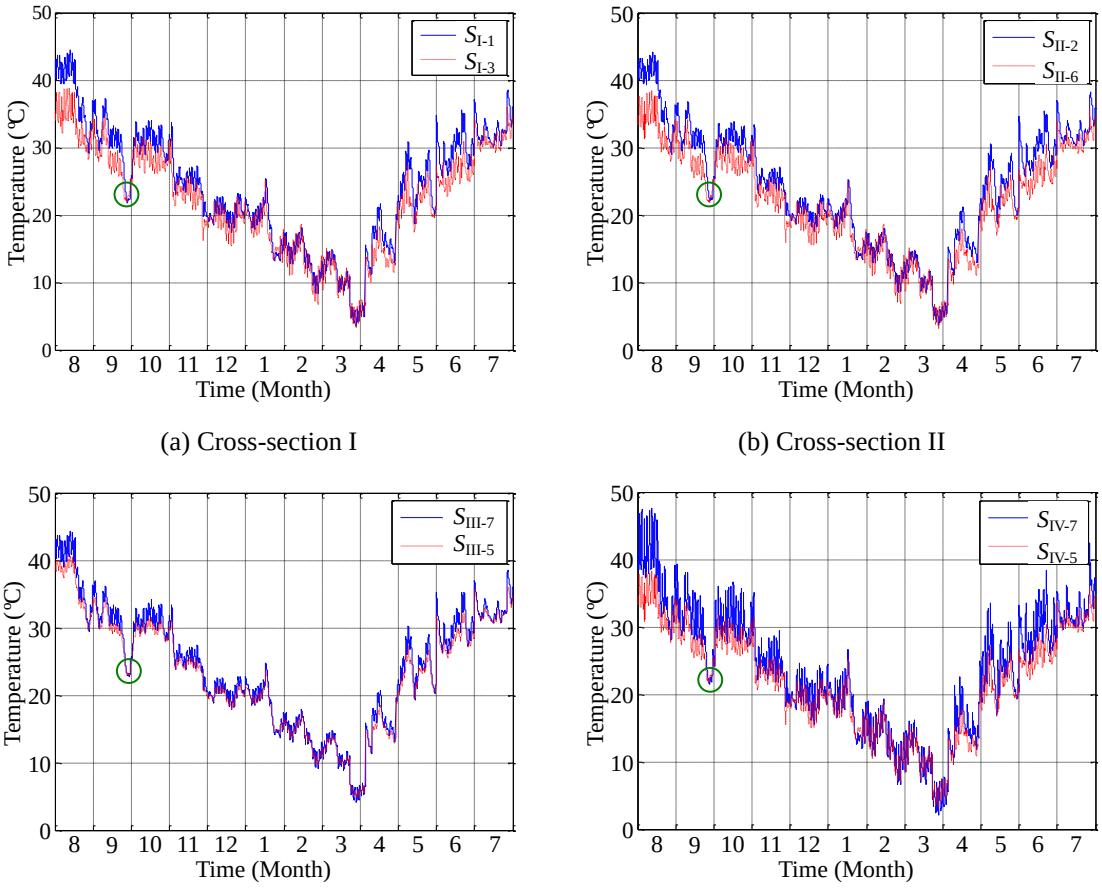

(a) Cross-section I

(b) Cross-section II

(c) Cross-section III

(d) Cross-section IV

Fig. 4 Temperature time histories for cross-sections

The comparison of the four figures reveals that all temperatures exhibit coincident variation tendency although they are measured from different points in the Jiubao Bridge. As denoted by circles in the four figures, temperatures at all measurement points experience a significant and almost simultaneous decrease due to cold air. The sensitivity of the temperature monitoring subsystem is validated, and the close correlation among temperatures at different points in the structure is revealed. Thus, temperatures in one cross-section can approximately represent the thermal loads of the entire bridge girder. In the temperature monitoring subsystem of the Jiubao Bridge, cross-section IV is carefully monitored. As shown in Fig. 3(d), the bottom plates, side plates and top plates of the steel box girder, diagonal braces, and concrete slabs are equipped by temperature sensors. Cross-section IV is located in the middle of the span and completely exposed to solar radiation. For brevity, the remainder of the paper focuses on temperature records for cross-section IV. The results in other cross-sections are employed for validation.

The comparison of the two temperature curves in the same cross-section reveals considerable temperature variation between the top and bottom cross-sections. In most cases, temperatures in the top cross-section are higher than the temperatures in the bottom cross-section. The considerable temperature variation may induce significant bending moments in vertical planes and internal thermal stress in cross-sections. For this reason, the characteristics of thermal gradients are discussed in Section 4.

3.2 Effective temperature

Generally, the temperature distribution in a cross-section is non-uniform for different heat properties of materials and different solar radiations. To describe the temperature in the entire cross-section, the effective temperature, which is defined by the weighted mean value of temperature distributed along the cross-section, is employed. According to its definition, the effective temperature T_e can be expressed as

$$T_e = \frac{\sum_{i=1}^{n} E_i \iint_{A_i} T_i(x,y)dxdy}{\sum_{i=1}^{n} E_i A_i} \tag{1}$$

where E_i represents the Young's modulus of subarea A_i; A_i denotes the ith subarea in the cross-section associated with temperature sensor S_i; $T_i(x,y)$ is the two-dimensional temperature over the subarea A_i; and x and y represent the horizontal axis and the vertical axis, respectively, of the cross-section. Dividing the cross-section into subareas is a complex problem. Taking cross-sections III as an example, the concrete slab and the steel box girder are treated separately for their different Young's moduli. The concrete slab is divided into three subareas from the midpoint between $S_{\text{III-1}}$ and $S_{\text{III-2}}$ and the midpoint between $S_{\text{III-2}}$ and $S_{\text{III-3}}$. Similarly, using the midpoint between $S_{\text{III-7}}$ and $S_{\text{III-8}}$ and the midpoint between $S_{\text{III-8}}$ and $S_{\text{III-5}}$ in the vertical direction, the steel box girder is divided into three layers. The top layer is belonged to the temperature sensor $S_{\text{III-7}}$, and the bottom layer is belonged to the temperature sensor $S_{\text{III-5}}$. The middle layer is divided into three subareas like the concrete slab.

The effective temperatures in cross-sections III and IV are calculated and illustrated in Fig. 5. In cross-sections III and IV, the effective temperatures show a similar variation tendency with

point temperatures. The effective temperature also changes with the seasons with the highest temperatures during the summer and the lowest temperatures during the winter. The highest effective temperatures in cross-section III and cross-section IV are 46.3℃ and 43.5℃, respectively. The lowest effective temperatures in cross-section III and cross-section IV are 3.4 ℃ and 3.2 ℃, respectively. The yearly effective temperature variation in cross-section III and cross-section IV are 42.9℃ and 40.3℃, respectively. This large temperature variation may result in a large longitudinal displacement in the bridge girder, which presents a challenge for the expansion joints and bearings.

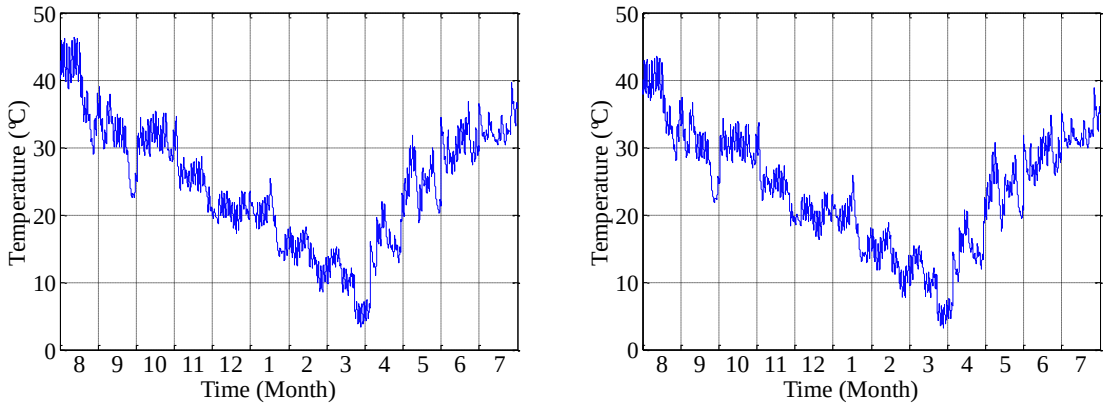

(a) Cross-section III (b) Cross-section IV

Fig. 5 Effective temperatures in the cross-sections

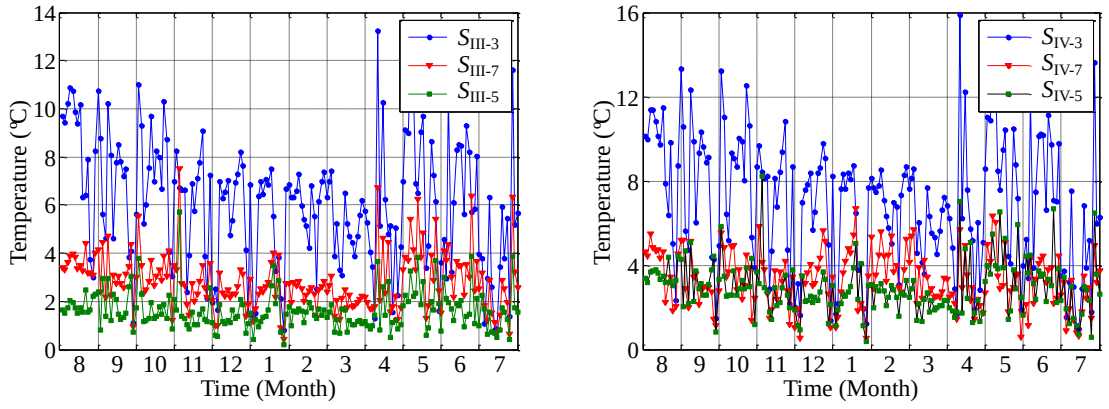

(a) Cross-section III (b) Cross-section IV

Fig. 6 Daily temperature variation for the cross-sections

3.3 Daily temperature variation

The daily temperature variation, which produces high-cycle expansion and contraction of structural components and opening and closing of cracks, may accelerate structural deterioration. The daily temperature variation for different points in cross-sections III and IV are computed and displayed in Fig. 6. Compared with point temperatures and effective temperatures, the daily temperature variation has no relationship with time. Thus, the air temperature is not the only factor that dominates the daily temperature variation. When comparing the three curves of daily temperature variation in cross-section III, the daily temperature variation for S_{III-3}, which is located in the concrete slab, is significantly larger than the daily temperature variation for S_{III-7} and S_{III-5}, which is located in steel, and the daily temperature variation for S_{III-7} is higher than the daily temperature variation for S_{III-5}. The same phenomenon is also observed in cross-section IV. Therefore, the findings conclude that the locations closer to the top surface of the cross-section experiences a greater daily temperature variation and concrete experiences a greater daily temperature variation than steel.

4. Thermal gradients in cross-sections

To satisfy the demands of passing vehicles and convenient construction, cross-sections of most bridge girders are designed as statically indeterminate structures. Thermal gradients induced by non-uniform solar radiation and heat exchange may cause significant thermal stress in these cross-sections, which has a more adverse influence on bridge performance than effective temperatures in some cases. Therefore, the thermal gradient is also a critical thermal load that must be considered in bridge design and evaluation. According to different effects, thermal gradients can be divided into a longitudinal thermal gradient that considers the relative deformation of an entire bridge, a vertical thermal gradients that results in supplementary internal axial forces and bending moments in vertical plane when the section ends are restrained, and a horizontal thermal gradient that induces secondary internal axial forces and bending moments in the horizontal plane if the deformation is constrained. In this section, the thermal gradients in the Jiubao Bridge are discussed.

4.1 Time history of thermal gradients

4.1.1 Longitudinal thermal gradients

Longitudinal thermal gradients between cross-section I and cross-section IV, which are located in the north approach bridge and the south approach bridge, respectively, are computed. The results are plotted in Fig. 7. Fig. 7(a) shows the thermal gradient between S_{I-1} and S_{IV-7}, which are both located on top of the box girder, and Fig. 7(b) shows the thermal gradient between S_{I-3} and S_{IV-5}, which are both located on the bottom of the box girder. The longitudinal thermal gradients randomly change and have no seasonal correlation. The two cross-sections that are separated by a distance of 810 m, but the maximal thermal gradient is 1.5℃. Thus, the longitudinal thermal gradient in the Jiubao Bridge can be neglected. The rationality of using the temperature of one cross-section to represent the temperatures of the entire bridge is again validated.

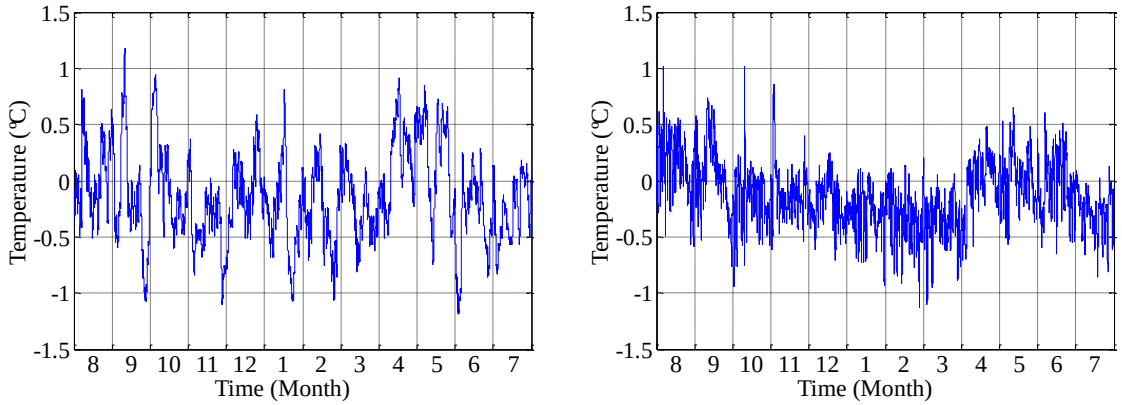

(a) Top (b) Bottom

Fig. 7 Longitudinal thermal gradients between cross-section I and cross-section IV

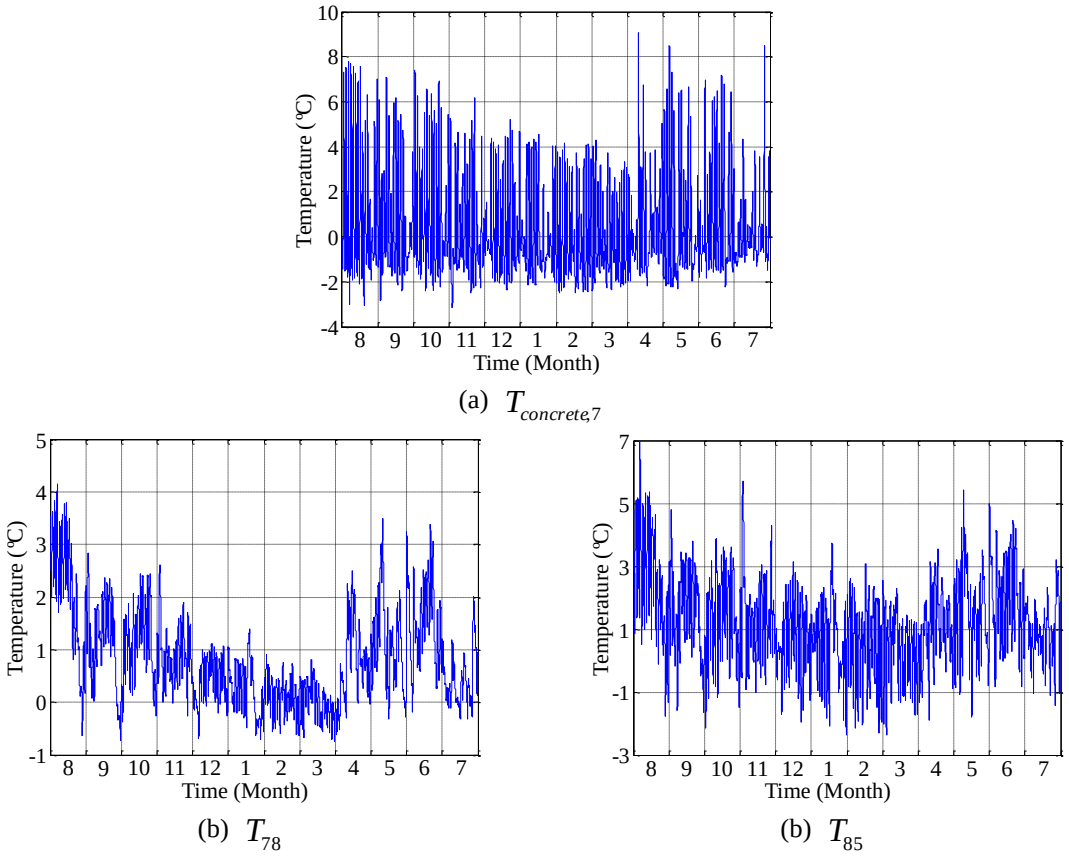

(a) $T_{concrete,7}$

(b) T_{78} (b) T_{85}

Fig. 8 Vertical thermal gradients in cross-section IV

4.1.2 Vertical thermal gradients

Vertical gradients in cross-section IV are shown in Fig. 8. The samples in Fig. 8(a) are obtained from the data, which are equal to the average values of $S_{I\text{-}1}$ and $S_{IV\text{-}2}$, subtracted the temperatures of $S_{IV\text{-}7}$. In the remaining two figures, T_{ij} represents the temperature variation between the ith temperature sensor and the jth temperature sensor. For example, T_{78} represents the temperature variation between $S_{IV\text{-}7}$ and $S_{IV\text{-}8}$. The vertical gradient and the longitudinal gradient are time-independent, as shown in Fig. 8. Because the surface of the concrete slab is completely exposed to solar radiation and is frequently encounters the friction of vehicle wheels, the temperatures in the concrete slab are distinctly higher than the temperatures in the top of the steel box girder, as displayed in Fig. 8(a). The maximal value is 9.1℃. Both point $S_{IV\text{-}7}$ and point $S_{IV\text{-}8}$, are located in the steel box girder and have no direct heat exchange with external air; thus, the thermal gradient T_{78} is relatively small. Conversely, the point of $S_{IV\text{-}5}$ engages in rapid heat exchange with the air beneath the box girder. The thermal gradient T_{85} is significant and its maximal value is 7.0℃. The vertical gradient among different heights in the cross-section is notable and should be further investigated.

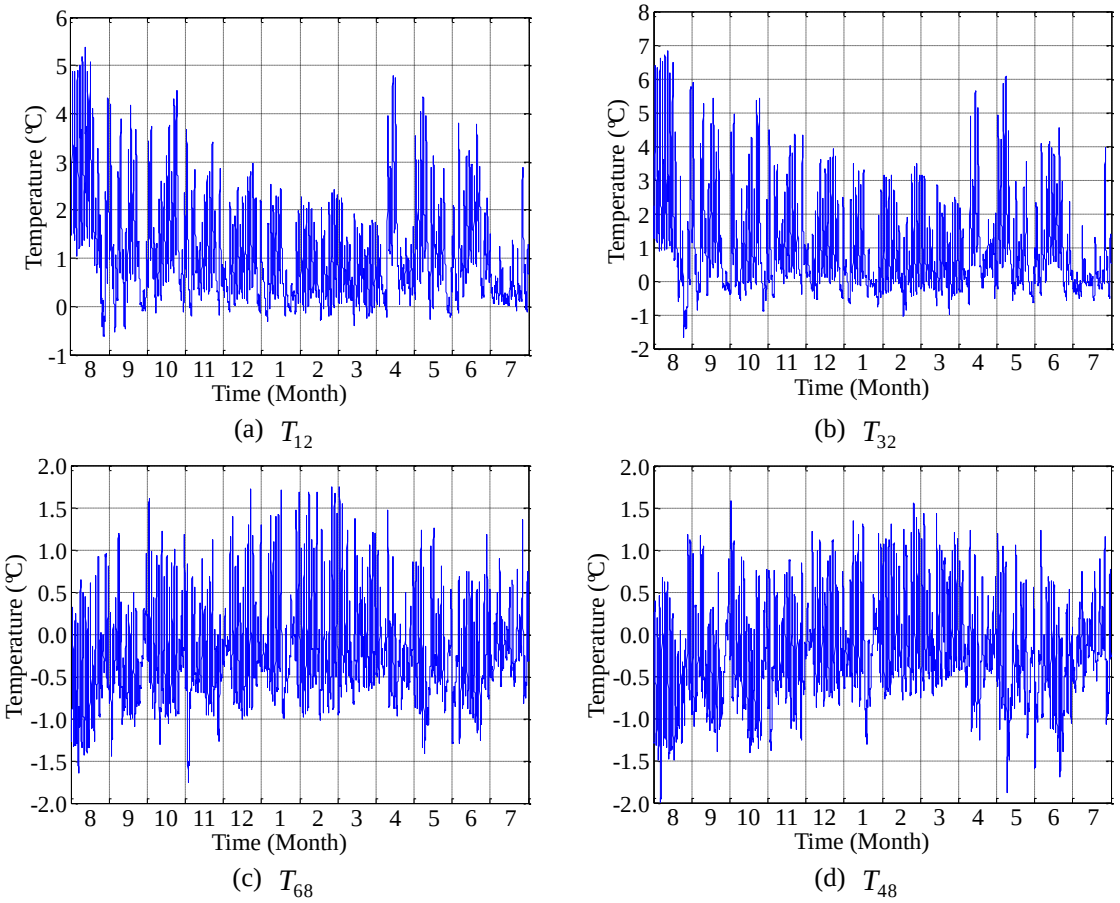

(a) T_{12} (b) T_{32}

(c) T_{68} (d) T_{48}

Fig. 9 Transversal thermal gradients in cross-section IV

4.1.3 Transversal thermal gradients

Fig. 9 displays transversal thermal gradients in different heights of cross-section IV. No time-dependent correlation is observed in these figures. The transversal thermal gradient in the concrete slab, as shown in Figs. 9(a) and 9(b), is considerable and the maximal value exceeds 6 ℃. The amplitudes of the transversal thermal gradients in the concrete slab are similar to the amplitudes of the vertical thermal gradients shown in Fig. 8(a). In most cases, the temperature of $S_{\text{IV-1}}$ and $S_{\text{IV-3}}$ are higher than the temperature of $S_{\text{IV-2}}$ because $S_{\text{IV-1}}$ and $S_{\text{IV-3}}$ are installed in the lanes where vehicles frequently pass. In addition to solar radiation, the friction between the wheel and the surface of the concrete slab increases the temperature in these locations. The $S_{\text{IV-2}}$ is located in the middle of the cross-section where no vehicles pass. Although the locations of $S_{\text{IV-6}}$ and $S_{\text{IV-4}}$ engage in rapid heat exchange with the air and the location of $S_{\text{IV-8}}$ experiences no heat exchange with air, this divergence does not induce a significant transversal thermal gradient in the middle height of the steel box girder, as shown in Figs 9(c) and 9(d). The maximal value does not exceed 2℃. By combining the four figures in Fig. 9, the transversal thermal gradient in the concrete slab is significant and should not be neglected and the transversal thermal gradient in steel box girder is small and can be disregarded. This phenomenon may be universal in wide bridge cross-sections because similar results were also obtained in another long-span bridge with concrete slabs supported by a flat steel box girder (Ding *et al*. 2012).

4.2 Statistical features of thermal gradients

The temperature distribution in cross-sections of bridge girders is primarily dominated by air temperature, solar radiation intensity, wind speed, and humidity, which change in a random manner. As a result, thermal gradients in bridge girders are random variables (Ho and Liu 1989). The statistical analysis is a powerful approach to capture the random features of random variables. Although the data for one year is minimal compared with the lifespan of a bridge, all thermal gradients have no relationship with time, as previously mentioned. The thermal gradients for one year yield the same probability distribution as the thermal gradients for the lifespan of a bridge. Then, the parametric distribution extracted from data provides an adequate representation of the statistical properties of thermal gradients during the entire lifespan. Among the variety of statistical properties, the probability density function (PDF) is a typical property. To obtain a proper PDF that describes a series of samples, two crucial steps, including the parameter estimation and the hypothesis testing, are required.

Among the different parameter estimation methods, the maximum-likelihood estimation (MLE), which was proposed by Gauss and spread by Fisher (1950), is an effective method and is employed in this paper. Assuming many independently measured temperature records $\{T_1, T_2, \ldots, T_n\}$ that obey an unknown probability distribution, where n is the number of independent records, the PDF of the unknown probability distribution can be represented by $f_0(\bullet)$. The PDF f_0 belongs to a certain family of distributions $f\{\bullet|\theta, \theta \in \Theta\}$ (where θ is the vector of parameters for this family), such as the normal distribution, the Poisson distribution, and the Rayleigh distribution. Then, the PDF f_0 becomes $f\{\bullet|\theta_0\}$, where θ_0 represents the true values of parameters that describe the actual distribution of temperature records. The purpose of parameter estimation is to obtain the estimator $\hat{\theta}$ that would be close to the true value θ_0 as possible. For all measured temperature records $\{T_1, T_2, \ldots, T_n\}$, their joint density function is

$$f\{T_1,T_2,\ldots T_n \mid \theta\} = \prod_{i=1}^{n} f\{T_i \mid \theta\} = L(\theta;T_1,T_2,\ldots T_n) \tag{2}$$

where ; represents the separation between the two input arguments: θ and the temperature records $\{T_1,T_2,\ldots,T_n\}$. In this equation, the temperature records $\{T_1,T_2,\ldots,T_n\}$ have fixed values and θ is the variable, which is allowed to vary freely. This function with variable θ is referred to as the likelihood function. In practice, the following logarithmic form is employed

$$\ln L(\theta;T_1,T_2,\ldots T_n) = \sum_{i=1}^{n} f\{T_i \mid \theta\} \tag{3}$$

Then, the partial differential of parameter θ_j in vector θ is given by

$$\frac{\partial[\ln L(\theta;T_1,T_2,\ldots T_n)]}{\partial\theta_j} = \frac{\partial[\sum_{i=1}^{n} f\{T_i \mid \theta\}]}{\partial\theta_j} \tag{4}$$

where θ_j denotes the jth parameter in the vector θ. Setting the right item of Eq. (4) to zero, the best estimator $\hat{\theta}$ can be solved.

By employing the MLE, a PDF for a type of thermal gradient can be estimated; however, the quality of the estimated PDF is unknown. The goodness of fit, which summarizes the discrepancy between the observed values and the values expected under the estimated model, is a reasonable metric for measuring how well the estimated PDF fits a set of observations. The goodness of fit is generally realized by the hypothesis testing, such as the Kolmogorov–Smirnov test (*K–S* test), and the Pearson's chi-squared test. In this paper, the *K–S* test, which tests whether two samples are drawn from identical distributions (Eadie 1971), is adopted. The *K–S* test employs the Kolmogorov–Smirnov statistic to quantify a distance between the actual cumulative distribution function (CDF) of samples and the estimated CDF. The Kolmogorov–Smirnov statistic for an estimated CDF of temperature records is defined as

$$D_k = \sup_T \left| F_k(T_i) - F(T_1,T_2,\cdots,T_n \mid \hat{\theta}) \right| \tag{5}$$

where $\sup_T$ represents the supremum of the set of distances, $F_k(T_i)$ denotes the cumulative probability of the temperature record T_i, and $F(T_1,T_2,\cdots,T_n \mid \hat{\theta})$ is the estimated CDF of temperature records. If all temperature records are obtained from the distribution $F(T_1,T_2,\cdots,T_n \mid \hat{\theta})$, the D_k yields to zero (Kotz and Nadarajah 2000).

After verifying the statistical features of the thermal gradients in the Jiubao Bridge, the generalized extreme value (GEV) distribution is selected to describe their probability distributions. Although the GEV distribution was developed within extreme value theory to combine the Gumbel, Fréchet and Weibull distributions, the PDF curve, which rapidly increases and slowly decreases, corresponds with the distribution of a large number of random variables. The PDF and the CDF of the GEV distribution are (Jenkinson 1955, Coles 2001)

$$f(x)=\begin{cases}\dfrac{1}{\sigma}[1+\xi(\dfrac{x-\mu}{\sigma})]^{(-1/\xi)-1}\exp\{-[1+\xi(\dfrac{x-\mu}{\sigma})]^{-1/\xi}\} & \xi\neq 0\\ \dfrac{1}{\sigma}\exp[-(\dfrac{x-\mu}{\sigma})]\exp\{-\exp[-(\dfrac{x-\mu}{\sigma})]\} & \xi=0\end{cases} \tag{6}$$

$$F(x)=\begin{cases}\exp\{-[1+\xi(\dfrac{x-\mu}{\sigma})]^{-1/\xi}\} & \xi\neq 0\\ \exp\{-\exp[-(\dfrac{x-\mu}{\sigma})]\} & \xi=0\end{cases} \tag{7}$$

where $f(x)$ and $F(x)$ represent the PDF and the CDF, respectively, of the random variable x, respectively, $\mu\in R$ is the location parameter, $\sigma>0$ denotes the scale parameter, and $\xi\in R$ is the shape parameter. When $\xi>0$, Eqs. (6) and (7) are valid for $x>\mu-\sigma/\xi$, whereas when $\xi<0$, they are only valid for $x<\mu-\sigma/\xi$. Then, the likelihood function with the logarithmic form of the GEV distribution is

$$\begin{aligned}\ln L(\theta;T_1,T_2,\ldots T_n)&=\ln L(\mu,\sigma,\xi;T_1,T_2,\ldots T_n)\\&=-n\ln\sigma-\sum_{i=1}^{n}[1+\xi(\frac{T_i-\mu}{\sigma})]^{-1/\xi}-(1+1/\xi)\sum_{i=1}^{n}\ln[1+\xi(\frac{T_i-\mu}{\sigma})]\end{aligned} \tag{8}$$

4.2.1 Vertical thermal gradients

Based on the criterion of the MLE, the parameters of the GEV distribution for the vertical thermal gradients at different heights are estimated. Fig. 10 shows the comparison between the probability densities of measured thermal gradients and the estimated PDFs. The two figures in Fig. 10 indicate that the estimated PDFs correspond with the probability densities of the measured data. A larger number of high thermal gradients make the probability density slowly decrease on the right side of the peak. A long tail exists in the PDF and extends to an extremely high value. The estimated PDFs of $T_{\text{concrete, 7}}$, T_{78} and T_{85} are listed in Table 1. By employing the *K-S* test, all estimated PDFs are acceptable at a significant level of 0.05.

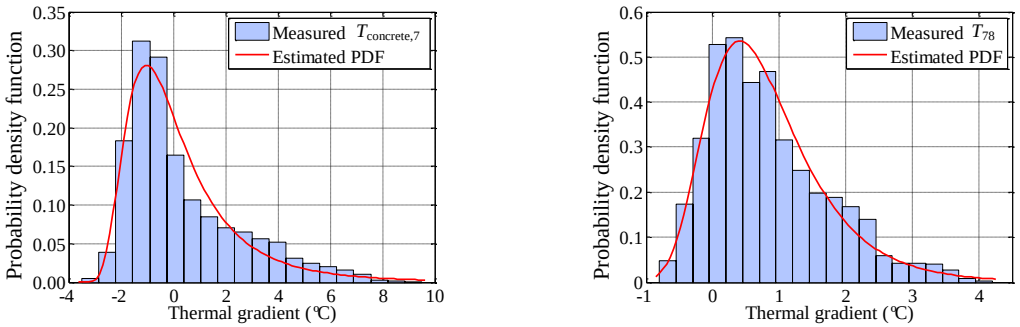

(a) $T_{concrete,7}$ (b) T_{78}

Fig. 10 Probability distribution of vertical thermal gradient in cross-section IV

Table 1 Estimated PDF of the vertical thermal gradient

Thermal gradient	PDF
$T_{concrete,7}$	GEV(-0.711,1.338,-0.771)
T_{78}	GEV(0.424,0.687,0.030)
T_{85}	GEV(0.717,1.306,-0.178)

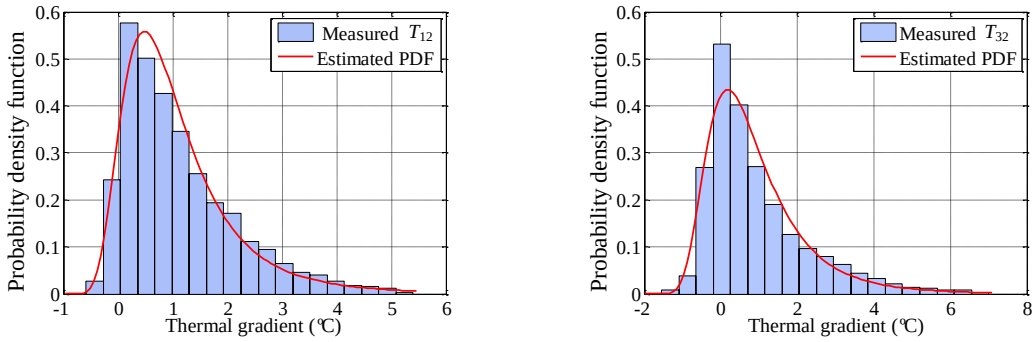

(a) T_{12} (b) T_{32}

Fig. 11 Probability distribution of transversal thermal gradient in cross-section IV

4.2.2 Transversal thermal gradients

Similar features such as long tails are revealed in the probability distribution of the transversal thermal gradients, including T_{12} and T_{32}. The PDF of these transversal thermal gradients are also estimated using the GEV distribution. The estimated PDFs show reasonable agreement with the measured results, as displayed in Fig. 11. Setting the significant level to 0.05, the *K-S* test indicates that the two estimated PDFs are acceptable. The estimated results are listed in Table 2.

4.2.3 Extreme value analysis of thermal gradients

In addition to the statistical model, which has the capability of determining the probability of different thermal gradient values, the extreme thermal gradient that may occur during the lifespan of a bridge is another critical parameter of bridge design. To define extreme values for design, the analysis of the thermal effects based on a proper probabilistic analysis of the thermal variables of bridge sections subjected to real climatic change is an effective and direct approach. However, the statistical analysis of field measurement data to obtain design values with an extended return period, such as 100 years, may be hampered by the problem of insufficient data records (Li *et al*. 2004). Extrapolation of available observations to determine extreme values beyond the period of record is an attractive option. The extreme value analysis (EVA), which emphasizes the behaviors of extreme observations instead of the complete sample population, enables the generalization of the return periods of extreme events and has been extensively applied in various engineering fields where extreme values are important (Castillo 1988, Roberts-Wollman *et al*. 2002, Castillo *et al*. 2005, Park and Sohn 2006, Adlouni *et al*. 2007). In this paper, EVA is employed to evaluate extreme thermal gradients, with the objective of estimating the magnitudes of the thermal variables within a specific return period.

Table 2 PDF of the transversal thermal gradient

Thermal gradient	PDF
T_{12}	GEV (0.593,0.668,0.180)
T_{23}	GEV (0.292,0.854,0.139)

If given samples of maxima or minima from the original observations, an EVA attempts to parametrically fit the data to one of the three limiting distributions, namely, the Gumbel distribution, the Weibull distribution, and Frechet distributions (Ni *et al*. 2007, Li *et al*. 2004). Jenkinson (1955) proved that the three distributions can be formulated as a generalized extreme value distribution, as represented by Eq. (6). Therefore, the GEV distribution is adopted in this study. The estimating distribution models are used to extrapolate extremes with a specified return period that is longer than the period of the observations. To maintain homogeneity and stochastic independence of the extreme samples, the samples of the maximal thermal gradients within selected time blocks of 24 hours are constructed. Consequently, EVA is performed using the block-reduced samples instead of 10-min average thermal gradients. As a result, the extreme thermal gradient T_W with a return period of W years can be estimated by applying the following equation

$$T_W = \begin{cases} \mu + \dfrac{\sigma}{\xi}\{1-[-\ln(1-p)]^{\xi}\} & \xi \neq 0 \\ \mu - \sigma \ln[-\ln(1-p)] & \xi = 0 \end{cases} \tag{7}$$

where $p = 1/vw$ denotes the probability of the occurrence of an extreme thermal gradient during the return period of W years and v is the number of time block units in which a one year span is divided. In this paper, the maximal values of each day are selected for the EVA; v is 365.

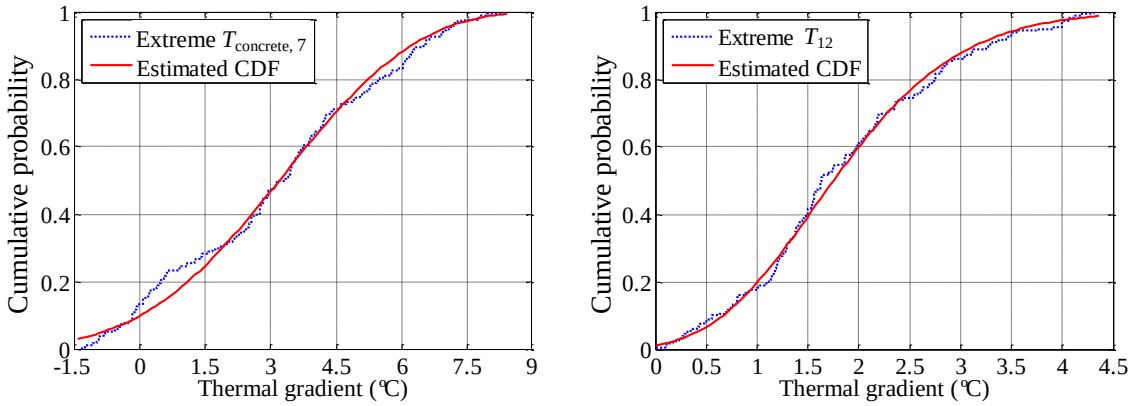

(a) $T_{concrete,7}$ (b) T_{78}

Fig. 12 The extreme distribution of thermal gradient in cross-section IV

Adopting the MLE and the *K–S* test with a significant level of 0.1, the parameters of the GEV distribution for daily extreme thermal gradients are estimated. The acceptable GEV distribution and the distribution of the measured daily extreme thermal gradients are both plotted in Fig. 12 for comparison. The estimated CDF agrees well with the monitored results.

The extreme thermal gradients in cross-section IV with return periods of 50 years and 100 years are predicted. For validation, the extreme values of the thermal gradients in cross-section III are also computed using the same approach. The almost equivalent extreme values of the thermal gradients in cross-section IV and cross-section III verify the reliability of the predicted results. The extreme vertical thermal gradient between the top surface and the bottom surface of cross-section IV with a return period of 50 years is 28.9℃. The extreme transversal thermal gradient with a return period of 50 years is 10.2℃, which is more than one third of the total vertical thermal gradient. The considerable thermal gradient in the vertical direction and the horizontal direction may induce significant thermal stress in the cross-section, which will degenerate the performance of the entire bridge. Combing the results in cross-section IV with the results in cross-section III, the profiles of the vertical thermal gradient in the Jiubao Bridge with return periods of 50 years and 100 years are plotted in Fig. 13. Unfortunately, the profiles of the transversal thermal gradient cannot be obtained due to insufficient temperature sensors in the cross-section. The profiles can provide a reference for the condition evaluation of this bridge and the structural design of other bridges with similar geometric configurations.

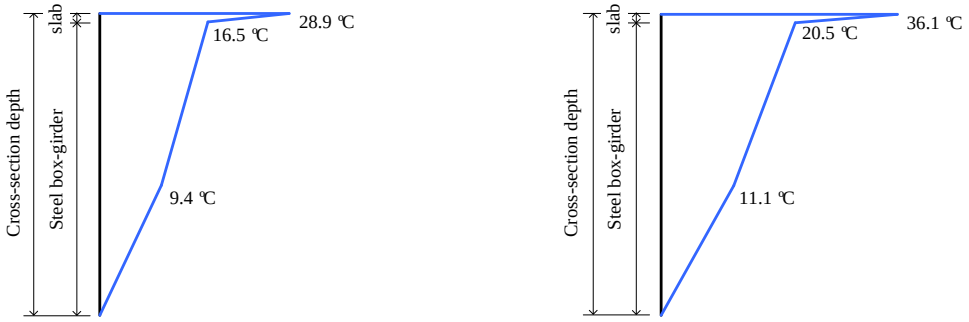

(a) 50 year return period (b) 100 year return period

Fig. 13 Profiles of the vertical thermal gradient in the Jiubao Bridge

Table 3 Extreme thermal gradient in cross-sections IV and III (unit: ℃)

Thermal gradient	Extreme values			
	Cross-section IV		Cross-section III	
	50 years	100 years	50 years	100 years
$T_{concrete,7}$	12.4	15.6	12.1	15.4
T_{78}	7.1	9.4	7.0	9.2
T_{85}	9.4	11.1	8.8	10.7
T_{12}	8.9	10.7	8.4	10.9
T_{23}	10.2	12.3	9.9	11.1

5. Conclusions

Thermal loads, especially the three-dimensional thermal gradients, are critical parameters that must be considered in the evaluation of structural health and in designing structural components. A large number of innovative bridges with extraordinary geometric configurations and combinations of different materials have been constructed in complex climatic conditions. As a result, the temperature distribution in these bridges significantly differs from previous findings. The SHM system, which can monitor temperatures in real time, provides a powerful approach to understand thermal features in a bridge. Based on temperature data for one year recorded by the SHM system installed on the Jiubao Bridge, three-dimensional gradients are investigated. Because of the negligible longitudinal thermal gradients, the vertical gradients and transversal gradients in cross-section IV can represent that in all other cross-sections of this bridge. Some conclusions are drawn as follows:

(1) The point temperatures measured from independent points on the Jiubao Bridge and the effective temperatures in the cross-sections are high in the summer and low in the winter; both have strong relationships with time. The highest temperature in the bridge is 50.0℃, and the maximum yearly temperature variation is 48.3℃. The considerable temperature variation may induce notable longitudinal displacement in the bridge, which should be addressed during bridge maintenance. The daily temperature variation is time-independent and randomly varies. The location, where is close to the top surface of the cross-section, exhibits greater daily temperature variation.

(2) All thermal gradients in three directions have no correlation with the seasons. The longitudinal thermal gradient is small and can be neglected in the entire bridge girder. The vertical thermal gradients among different levels in a cross-section are notable. The maximal temperature variation between the top of the concrete slab and the bottom of the concrete slab is 9.1℃, and the maximal temperature variation between the top and the bottom steel box girder is approximately 14.5℃. The transversal thermal gradient in the concrete slab corresponds with the vertical thermal gradient in the concrete slab and its maximal value exceeds 6 ℃. However, the transversal thermal gradient in the steel box girder is not distinct.

(3) Both the vertical thermal gradient and the transversal thermal gradient follow the GEV distribution. The parameters of the GEV distributions of different thermal gradients can be properly estimated by the MLE and examined by the *K-S* test with a confidential level of 0.05. The extreme values of the vertical thermal gradient with return periods of 50 years and 100 years are 28.9℃ and 36.1℃, respectively, and the extreme values of the transversal thermal gradient with a return period of 50 years and 100 years are 10.2℃ and 12.3℃, respectively. The extreme transversal thermal gradient is more than one third of the total vertical thermal gradient. The profiles of the vertical thermal gradient for the Jiubao Bridge with return periods of 50 years and 100 years can provide a reference for the condition evaluation of this bridge and the structural design of similar bridges.

Acknowledgments

This research work was jointly supported by the 973 Program (Gran no. 2015CB060000), the National Natural Science Foundation of China (Grant nos. 51121005, 51308186, 51222806), the

Fok Ying Tong Education Foundation (Grant no. 141072), the Specialized Research Fund for the Doctoral Program of Higher Education (Grant No. 20130041110031), and the Science Fund for Distinguished Young Scholars of Dalian.

References

Castillo, E. (1988), *Extreme Value Theory in Engineering*, Elsevier, Amsterdam, North-Holland.

Castillo, E., Hadi, A.S., Balakrishnan N, and et al. Extreme value and related models with applications in engineering and science, Wiley, Hoboken, N.J., 2005 Hadi, A.S., Balakrishnan, N. and Sarabia, J.M. (2005), Extreme Value and Related Models With Applications in Engineering and Science, Wiley, Hoboken, NJ, USA.

Coles, S. (2001), *An Introduction to Statistical Modeling of Extreme Values*, Springer-Verlag, New York, NY, USA.

Ding, Y., Zhou, G., Li, A. and Wang, G. (2012), "Thermal field characteristic analysis of steel box girder based on long-term measurement data", *Int. J. Steel. Struct.*, **12**(2), 219-232.

Duffie, J.A. and Beckman, W. A. (2013), *Solar Engineering of Thermal Processes*, John Wiley & Sons, New York, NY, USA.

Eadie, W.T., Drijard, D., James, F.E., Roos, M. and adoulet B.S. (1971), S*tatistical Methods in Experimental Physics*, 269-271, Amsterdam, North-Holland.

El Adlouni, S., Ouarda, T.B.M.J., Zhang, X., Roy, R. and Bobée, B. (2007), "Generalized maximum likelihood estimators for the nonstationary generalized extreme value model", *Water. Resour. Res.*, **43**(3), 737-744.

Elbadry, M.M. and Ghali, A. (1983), "Temperature variations in concrete bridges", *J. Struct. Eng. - ASCE*, **109**(10), 2355-2374.

Fisher, R.A. (1950), *On the Mathematical Foundations of Theoretical Statistics*, John Wiley & Sons, New York, NY, USA.

Fu, H.C., Ng, S.F. and Cheung, M.S. (1990), "Thermal behavior of composite bridges", *J. Struct. Eng - ASCE*, **116**(12), 3302-3323.

Ho, D. and Liu, C. H. (1989), "Extreme Thermal Loadings in Highway Bridges", *J. Struct. Eng. - ASCE*, **115**(7), 1681-1696

Im, C.K. and Chang, S.P. (2004), "Estimating extreme thermal loads in composite bridge using long-term measured data", *Int. J. Steel. Struct.*, **4**(1), 25-31.

Jenkinson, A.F. (1955), "The frequency distribution of the annual maximum (or minimum) values of meteorological elements", *Q. J. Roy. Meteor. Soc.*, **87**, 145-158.

Kotz, S. and Nadarajah, S. (2000), *Extreme Value Distributions-Theory and Applications*, Imperial College Press, London, United Kingdom.

Lee, J.H. (2012), "Investigation of extreme environmental conditions and design thermal gradients during construction for prestressed concrete bridge girders", *J. Bridge. Eng.*, **17**(3), 547-556.

Li, D., Maes, M.A. and Dilger, W.H. (2004), "Thermal design criteria for deep prestressed concrete girders based on data from Confederation Bridge", *Can. J. Civil. Eng.*, **31**(5), 813-825.

Mirambell, E. and Aguado, A. (1990), "Temperature and stress distributions in concrete box girder bridges", *J. Struct. Eng. - ASCE*, **116**(9), 2388-2409.

Moorty, S. and Roeder, C.W. (1992), "Temperature-dependent bridge movements", *J. Struct. Eng. - ASCE*, **118**(4), 1090-1105.

Ni, Y.Q., Hua, X.G., Wong, K.Y. and Ko, J.M. (2007), "Assessment of bridge expansion joints using long-term displacement and temperature measurement", *J. Perform. Constr. Fac.*, **21**(2), 143-151.

Oesterle, R.G., Sheehan, M.J., Lotfi, H.R., Corley,W.G., and Roller, J.J. (2007), *Investigation of red mountain freeway bridge girder collapse*, CTL Group Project No. 262291, CTL Group, Skokie, IL.

Orgill, J.F. and Hollands, K.G.T. (1977), "Correlation equation for hourly diffuse radiation on a horizontal

surface", *Sol. Energy*., **19**(4), 357-359.
Park, H.W., and Sohn, H. (2006), "Parameter estimation of the generalized extreme value distribution for structural health monitoring", *Probabilist. Eng. Mech.*, **21**(4), 366-376.
Potgieter, I.C. and Gamble, W.L. (1983), *Response of Highway Bridges to Nonlinear Temperature Distributions*, University of Illinois at Urbana-Champaign, Urbana-Champaign, Illinois, USA.
Roberts-Wollman, C.L., Breen, J.E. and Cawrse, J. (2002), "Measurements of thermal gradients and their effects on segmental concrete bridge", *J. Bridge. Eng*., **7**(3), 166-174.
Xia, Y., Chen, B., Zhou, X. and Xu, Y.L. (2013), "Field monitoring and numerical analysis of Tsing Ma Suspension Bridge temperature behavior", *Struct. Control. Health*., **20**(4), 560-575.
Xia, Y., Hao, H., Zanardo, G. and Deeks, A.J. (2006), "Long term vibration monitoring of a RC slab: temperature and humidity effect", *Eng. Struct.*, **28**(3), 441-452.
Xu, Y.L., Chen, B., Ng, C.L., Wong, K.Y. and Chan, W.Y. (2010), "Monitoring temperature effect on a long suspension bridge", *Struct. Control. Health*., **17**(6), 632-653.
Ye, X.W., Ni, Y.Q., Wong, K.Y. and Ko, J M. (2012), "Statistical analysis of stress spectra for fatigue life assessment of steel bridges with structural health monitoring data", *Eng. Struct*., **45**, 166-176.
Ye, X.W., Ni, Y.Q., Wai, T.T., Wong, K.Y., Zhang, X.M. and Xu, F. (2013), "A vision-based system for dynamic displacement measurement of long-span bridges: algorithm and verification", *Smart Struct. Syst*., **12**(3-4), 363-379.
Zhou, G.D. and Yi, T.H. (2013), "Thermal load in large-scale bridges: a state-of-the-art review", *Int. J. Distrib. Sens. N.*, Article ID 217983, 1-17.
Zuk, W. (1965), "Thermal behaviour of composite bridges-insulated and uninsulated", *Highway Res. Record*, **76**, 231-253.